

PIV ANALYSIS OF TURBULENT FLOW IN A MICRO-CHANNEL

SŁAWOMIR BŁOŃSKI
TOMASZ A. KOWALEWSKI

*Institute of Fundamental Technological Research, Polish Academy of Sciences, Warsaw, Poland
e-mail: tkowale@ippt.gov.pl*

Turbulent flow of water in a short 0.4 mm high micro-channel of an emulsifier is investigated experimentally using a micro-PIV technique and compared with numerical predictions. The micro-flow measurements are based on epi-fluorescence illumination and high-speed imaging. Velocity fields obtained from the measurements and direct numerical simulations indicate that flow turbulization is delayed and develops only at the outlet region of the micro-channel.

Key words: micro-channel, micro-PIV, turbulence

1. Introduction

Turbulent flow is commonly used for the emulsification process in industrial applications. The process is very effective but produces relatively non-homogenous emulsions. It is usually assumed that the final droplet size is related to turbulent kinetic energy of the flow.

The main aim of the present study is to investigate the flow structure using the micro-PIV experimental technique for the flow in a flat, continuous stream homogeniser (Błoński *et al.*, 2007; Kowalewski *et al.*, 2006). The micro-PIV technique allows for full-field analysis of the velocity fields in a narrow gap formed by rapid contraction of the emulsifier, offering a unique opportunity to verify assumptions on the development of the turbulent flow.

In the last decade, micro particle image velocimetry (micro-PIV), as a non-intrusive technique for measuring flow fields, has been successfully adapted for measuring flow fields within micro fluidic devices with micron-scale resolution, e.g. Meinhart *et al.* (2000). For higher temporal resolution, Shinohara *et al.* (2004) used a high-speed micro-PIV technique by combining a high-speed camera and a continuous wave laser in order to investigate transient phenomena

in micro-fluidic devices. The micro-PIV technique refers to the application of PIV to measure velocity fields of fluid motion with length scales of the order of 100 micrometers and with spatial resolution of individual velocity measurements of the order of 1-10 micrometers. Due to small dimensions, the light sheet technique, typical for macro-scale PIV, cannot be applied for flow illumination, and the whole investigated volume is flooded with light. Images of individual tracers, necessary for PIV evaluation, are obtained by taking advantage of fluorescence, removing by appropriate filters diffused light originating from the bulk illumination.

Fundamentals of the micro-PIV method were established by Santiago *et al.* (1998), who used a mercury arc lamp to continuously illuminate 300 nm fluorescent tracers. Using a microscope, an image intensified CCD camera and narrow wavelength optical filter, they obtained discrete images of fluorescent tracers. Correlation analysis was then applied to the particle image field, producing a regularly spaced velocity field. The flow fields measured under the microscope is characterized by high relative velocity due to large spatial magnification of recorded tracer displacements. It limits the magnitude of velocity to about 0.1 mm/s for epi-fluorescent systems equipped with a mercury lamp. A double pulsed Nd:Yag laser applied for illumination allows for a very short illumination time (5 ns), enormously extending the velocity range of evaluated under a microscope flow fields.

The majority of investigations performed in micro-channels are limited to steady, low Reynolds number flows. It is mainly due to experimental constraints, which demand high speed imaging systems and high pressures to enforce the flow. The present paper reports on micro-PIV measurements performed for flow velocities of several m/s in a channel of only 400 μm height. To our knowledge, there are very few reports on micro-flow measurements in this range of parameters. Recently Li and Olsen (2006) investigated the transition to turbulent flow in a micro-channel. Their experiment rejects earlier suggestions of possible early transition to turbulence in micro-channel flows. In fact, the main result of our paper claims even possible delayed transition to turbulence. At high Reynolds number ($\text{Re} = 6770$), the flow measured within our short micro-channel remains quasi-laminar.

2. Experiment

The flow of pure water was studied in a flat model of an emulsifier. It is a two dimensional substitute of the central cross-section of the axially-symmetric emulsifier thoroughly investigated in a separate study (Brenn, 2005; Steiner *et al.*, 2006). The emulsifier consists of a small channel formed between two

glass plates and a triangular processing element creating rapid flow contraction (Fig. 1). The flat geometry and two glass windows permit application of optical methods for measuring flow velocity fields (PIV method).

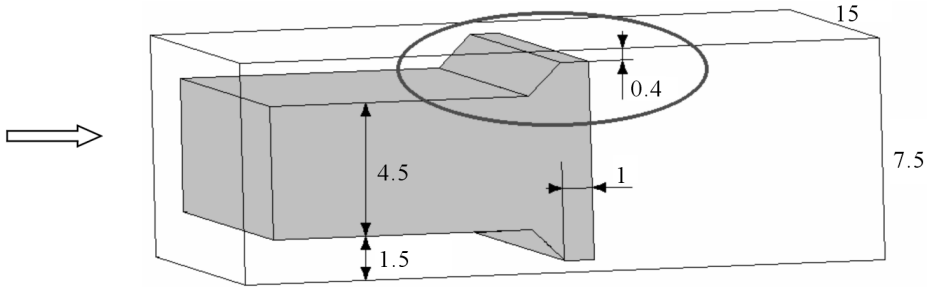


Fig. 1. Geometry of the processing element of the emulsifier model and location of the analysed micro-channel. The micro-channel size: height 0.4 mm, width 15 mm and length 1 mm. The flow inlet is indicated by an arrow: the inlet and outlet heights are 1.5 mm, 7.5 mm, respectively

Dimensions of the gap between the glass plates and processing element (triangular obstacle) are 0.4 mm in height, 1 mm in length and 15 mm in width. The processing element forms two inlets of a rectangular shape (upper and lower); they are 15 mm wide and 1.5 mm high. After passing the gap, the flow geometry abruptly expands, filling 15 mm wide and 7.5 mm high outlet. The total length of the inlet segment is 97.5 mm and the length of the outlet segment is 78.5 mm. These physical dimensions were implemented as a computational domain used to simulate 3D flow in the emulsifier. However, experimental and numerical data presented in the following, deal with the central cross-section of the micro-channel and a short part of the outlet. The inlet and outlet of the channel are connected through 8 mm tubes with the liquid supply system. Pressurized nitrogen was used to pump the liquid through the homogeniser to the collecting bottle. The flow rate was set by varying the reservoir pressure and using the system of valves. The exact value of the flow rate was obtained by measuring the time necessary to fill up a calibrated quantity in the collecting bottle. The flow rate used in the experiment was $Q_V = 0.204 \text{ dm}^3/\text{s}$. The same flow rate was used in the numerical models.

The flow Reynolds number is defined as

$$\text{Re} = \frac{\rho l V}{\mu}$$

where ρ , μ indicate density and viscosity of water, l , V – height of the channel and mean flow velocity.

For the given flow rate, the average flow velocity in the 8 mm inlet tube is nearly 1 m/s, and it increases to about 17 m/s in the gap of 0.4 mm height.

Hence, the characteristic Reynolds number based on the inlet tube diameter and the micro-channel height varies from about 8000 to 6770, respectively. These values are high enough to expect a transition to the turbulent flow regime.

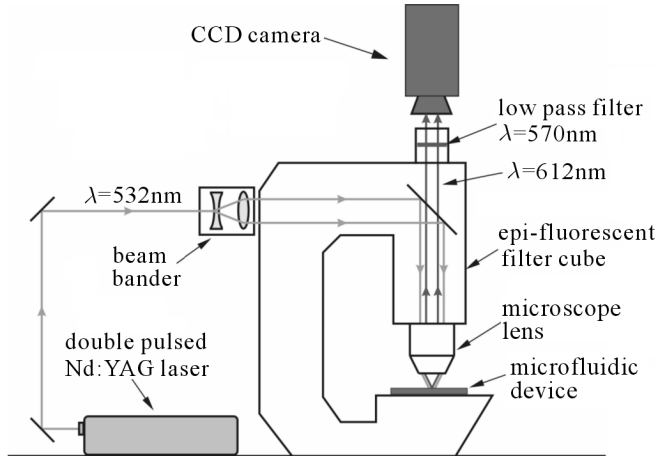


Fig. 2. Scheme of the micro-PIV experimental set-up. The investigated channel is illuminated by Nd:Yag laser through the microscope lens. The same lens is used for imaging a selected flow plane, recorded by the CCD camera

The main part of the experimental set-up consists of a microscope, an emulsifier with transparent windows, a laser light source and a digital camera (Fig. 2). The flow was examined using an epi-fluorescence microscope (Nikon Eclipse 50i) equipped with the $10\times$ (NA 0.3/WD 17.30 mm) microscopic lens. The flow observed under the microscope is characterized by large relative displacements; therefore application of high-speed recording techniques becomes essential. In our case, the image width of 1280 pixels corresponds, for the highest magnification ratio, to the object dimension of 0.172 mm. With the flow velocity of 1 m/s, the illumination time necessary to freeze the motion is below 100 ns. Such a short illumination time was achieved by using a pulsed light of Nd:YAG laser, delivering 30 mJ energy at 532 nm wavelength (New Wave Research, Inc.). For recording the images, a high-resolution (1280×1024 pixels) 12bit *PCO SensiCam* camera was used. When coupled with the double pulse laser it permits acquisition of two images at the minimum time interval of 200 ns, exposition time of 5 ns, and about 3.75 Hz repetition rate. The PIV recording system installed on 3 GHz Pentium 4 computer with 3 GB RAM enabled us to acquire over 200 pairs of images during a single experimental run.

The micro-PIV measurements were performed for pure water seeded with fluorescent tracers, polystyrene spheres of $2\ \mu\text{m}$ in diameter (Duke Scientific

Inc.). The particle volumetric concentration was very low ($< 0.0001\%$ wt), hence they did not affect the flow structure. Particle Image Velocimetry (PIV) based on correlation of pairs of images was used to evaluate instantaneous velocity fields in the channel. Unlike typical PIV methods, the micro-PIV does not utilize a thin laser sheet to illuminate the seeding particles. The whole investigated volume was flooded with the laser light using a beam expander and the microscope objective (Fig. 2). Once the particles are exposed to 532 nm light (green) from the laser, they emit red light with the emission maximum at 612 nm, as specified by the supplier. The time-span in which particles continue to fluoresce after application of the laser pulse is of the order of nanoseconds, so motion induced blurring of the particles does not occur in the PIV images. Two low pass filters, mounted between the objective and the camera, only enable the fluorescent red light to pass, while preventing the green laser light to be detected by the camera. The micro-PIV images present well detectable bright spots of the seeding particles. Only particles being within the depth of focus are recorded. Particles that are out of focus add background noise, limiting the applicability of the technique to thin layers of the fluid (max. 10-15 μm).

The flow was illuminated and observed through the upper window of the channel. By traversing the field of observation in the horizontal and vertical direction, the position of the interrogated flow plane was selected. The vertical resolution depends on the depth of field of the objective. For the micro-PIV experiments performed using the $10\times$ objective, the vertical resolution was estimated to be 10 μm and each PIV measurement covered an area of about $0.7\text{ mm}\times 0.55\text{ mm}$. The horizontal resolution of the velocity field measurements for this objective was 0.5 μm . The accuracy of the velocity measurement depends on several experimental factors (quality of the images, seeding concentration, particle displacement) as well as on the vector evaluation procedure. Using in-house developed software and by evaluating a uniform, predefined flow of water through the micro-channel, the error of velocity measurement was estimated to be below 5%.

As results, five sets of velocity fields were obtained from the micro-PIV measurements – each of them at different locations within and behind the micro-channel (Fig. 3). The area interrogated by the PIV method was in all cases located in the mid-plane between side walls. In the coordinate system described in Fig. 3, the micro-channel extends from $x = -1\text{ mm}$ to 0. Measurements at positions P1 and P2 were obtained for the centre plane of the gap ($y = -0.2\text{ mm}$) and used to evaluate velocity profiles along the x -direction in the vicinity of the gap entrance and the gap exit. It extends from $x = -1.4\text{ mm}$ to $x = -0.7$ for the location P1 and from $x = -0.35\text{ mm}$ to $x = 0.35\text{ mm}$ for the location P2. Measurements at positions P3, P4 and P5 were performed for several y planes, changing the focal distance of the microscope from the

vicinity of the upper glass wall ($y = 0$) down to the centre plane of the outlet channel ($y = -3.75$ mm). It permitted us to evaluate development of the flow structure along the y -direction at three investigated locations, i.e. 1 mm, 3 mm and 8 mm behind the gap.

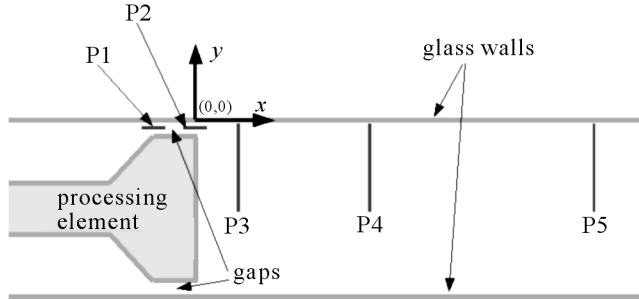


Fig. 3. Schematic drawing of the emulsifier with the coordinate system and locations where the velocity fields were measured by the micro-PIV method (P1-P5). The beginning of the coordinate system is placed at the exit edge of the processing element ($x = 0$) attached to the top wall ($y = 0$), and located in the symmetry-plane ($z = 0$). P1, P2 indicates PIV interrogation planes located in the mid-height of the gap ($y = -0.2$ mm) covering partly the gap inlet and outlet, respectively. P3-P5 indicate location of PIV interrogation planes used to measure velocity distribution from the top wall to the flow axis ($y = 0$ to $y = -3.75$ mm). They are located at distances $x = 1$ mm (P3), $x = 3$ mm (P4), and $x = 8$ mm (P5) from the gap exit

In order to quantify the turbulence in the channel, the ensemble-averaged velocity fields were calculated at each analysed location. For locations P1 and P2 (within the gap), the micro-PIV measurements were repeated up to hundred times at the same position. For locations P3, P4 and P5 (behind the gap) measurements were repeated 28 times for each of about 20 planes of selected channel depths. The velocity was averaged over the velocity field and then over all 28 measurements taken at the interrogated location P3-P5 (over 100 measurements at P1 and P2).

Velocity measurements performed at two positions P1 and P2 within the gap indicate that the flow through the gap is practically steady, no large temporal flow field fluctuations could be observed for these two locations. For position P1, the streamwise velocity of the flow rapidly increases from 8 m/s to 16 m/s (Fig. 4 – P1) in the vicinity of the entrance to the gap, but it remains steady in time. Despite high velocities flow seems to be laminar. Velocity measurements for location P2 (Fig. 4 – P2) show flow development in the vicinity of the gap exit. Just behind the gap, the streamwise flow velocity rapidly decreases from 18 m/s down to 16 m/s. Some initial spatial flow perturbation becomes visible here, indicating the beginning of transition to turbulence.

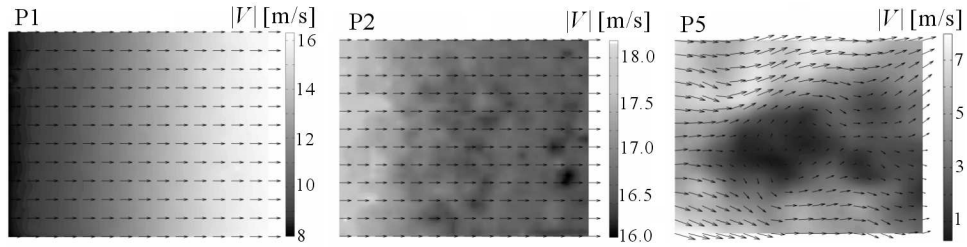


Fig. 4. Velocity vector field and velocity magnitude $|V|$ contours measured 0.2 mm below the top wall at the gap entrance (location P1), at the gap exit (P2), and 8 mm behind the gap (P5); image displays the velocity field for the area of $0.7 \text{ mm} \times 0.55 \text{ mm}$

The main reason of the observed flow acceleration and deceleration is the rapid change of the channel height in the vicinity of the processing element. The channel height converges from 1.5 mm before the gap down to 0.4 mm in the gap, and expands to 7.5 mm behind the gap. Due to the fluid acceleration and deceleration, strong shear stresses are produced in the flow. Shortly behind the processing element, the flow velocity apparently changes its character, both flow direction and velocity amplitude strongly vary in time (comp. Fig. 4 – P5).

The flow structure behind the processing element was analysed at three locations (P3, P4, and P5) along the x -axis, and for about 20 positions along the y -axis (comp. Fig. 3). At each position, the PIV velocity field was acquired for a small interrogation area of $0.7 \text{ mm} \times 0.55 \text{ mm}$, delivering nearly 10^6 individual vectors. In addition, measurements were repeated 28 times for the same location. Assuming homogeneity of the velocity field within the small area covered by the PIV measurement, the ensemble-averaged velocity and velocity fluctuations were evaluated at each interrogated position using a huge set of measured velocity vectors. These micro-PIV measurements were used to evaluate profiles of the time and space averaged x -component of velocity along the y -direction, i.e. channel height (Fig. 5).

The coordinate value $y = 0$ corresponds to the surface of the upper glass wall (comp. Fig. 3), and $y = -3.75 \text{ mm}$ to the plane of symmetry of the emulsifier. Symbols $\langle V_x \rangle$ indicate the mean values of the velocity x -component V_x . It is worth to note the high velocity "jet flow" present in the vicinity of the top wall. The reversal flow can be found closer to the channel symmetry plane indicated in the profiles as negative values of the flow velocity (comp. Fig. 5 – P5).

For evaluating turbulent characteristics of the flow field behind the processing element, the velocity fluctuations V'_x and V'_z were evaluated from the experimental data. The sum of their squared values was used to represent the turbulent kinetic energy (tke_{xz}) of the flow. It was obtained from both ava-

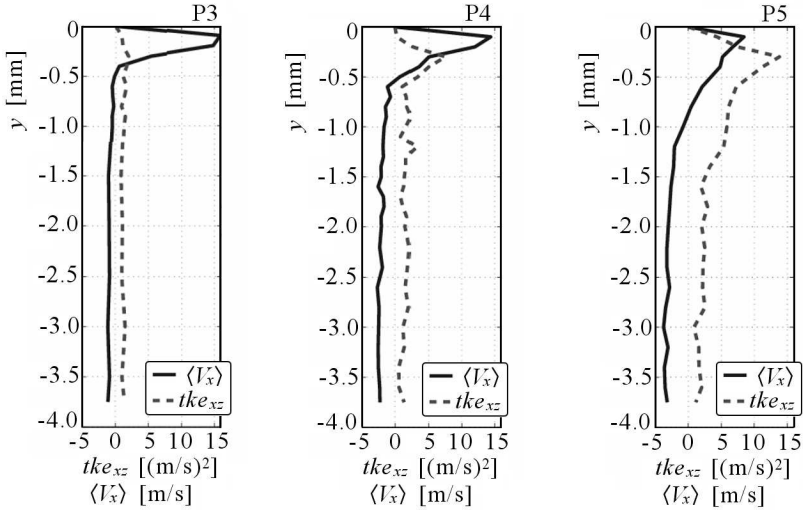


Fig. 5. The time-averaged x -component of the flow velocity $\langle V_x \rangle$ (solid line), and fluctuations tke_{xz} (dashed line) representing turbulent kinetic energy. Data obtained from micro-PIV measurements performed along the y -direction for locations P3, P4 and P5

ilable horizontal components of the velocity, however streamwise fluctuations were dominating in all investigated cases.

Figure 5 shows variation of tke_{xz} (dashed line), representing turbulent kinetic energy calculated from measurements performed at selected locations P3, P4 and P5. Profiles of tke_{xz} indicate that turbulent fluctuations emerge just behind the gap and persist along the x -direction. The tke_{xz} reaches its maximum about 0.3 mm below the glass wall. This is the region, where intense mixing occurs between high speed fluid arriving from the gap and low velocity recirculating flow behind the processing element. The peak value of the tke_{xz} is observed for the last interrogated position P5, i.e. about 8 mm from the gap.

3. Numerical simulations

Numerical simulations of the flow of water were done using CFD code *Fluent* (Fluent Inc.) (Błóński *et al.*, 2007). Two types of numerical simulations were performed. To evaluate flow fluctuations Direct Numerical Simulation (DNS) was performed by solving the Navier-Stokes equations without any turbulence model. In the separate computational runs, the averaged Navier-Stokes equations were solved using the k - ε turbulence model. These computations delivered the averaged flow structure and the turbulent dissipation rate in the

vicinity of the processing element (Brenn, 2005; Błoński *et al.*, 2007; Steiner *et al.*, 2006).

The DNS model allows one to obtain an accurate, unsteady solution to unmodified Navier-Stokes equations by resolving the whole range of spatial and temporal scales of the turbulence from the smallest dissipative scales (Kolmogorov scales) up to the integral scale associated with motions containing most of the kinetic energy. The numerical domain used in the simulations had to cover full 3D geometry of the physical channel. All the spatial scales of the turbulence had to be resolved in the computational mesh. Hence, a very fine mesh and small time steps were used.

A direct numerical simulation (DNS) performed with the classical finite volume code implemented in *Fluent* is time consuming and vulnerable. Nevertheless, it appeared that for the investigated geometry it was possible to obtain reasonable solutions reproducing typical for the turbulence flow characteristics. These results were compared with the outcome of the steady, average turbulence model, where the flow symmetry was assumed, and only one quarter of the model geometry was used for the computational domain.

The turbulent flow model assumes *a priori* that the flow is turbulent and properly described by the averaged variables using Reynolds hypothesis. The reliability of the simulation results depends on several empirical parameters assumed to be applicable to a specific flow configuration. The main advantage of using the average turbulence models is their computational efficiency. The computations were performed using the standard $k-\varepsilon$ model with default parameters and an enhanced wall treatment. These parameters and appropriate computational mesh were selected after performing several test calculations. The average model enables one to assume flow symmetry, therefore only one-quarter of the physical domain was implemented into the computational scheme, extremely improving computational efficiency.

In both computational models, the structural hexahedron mesh with a boundary layer was generated in the gap and in the vicinity of the processing element. The tetrahedron mesh was used in the remaining parts of the computational domain, reproducing all geometrical details of the emulsifier. Several mesh resolution tests were performed to identify the optimal mesh, being a compromise of the computational time and numerical accuracy. The most critical flow region is within the gap. The optimal mesh sought using the convergence grid index and applying mesh adaptation technique for the gap region was found for the turbulent model to consist of nearly 0.5 mln grid cells. For the DNS model, it was found that sufficient accuracy was obtained for the gap mesh of $50 \times 60 \times 50$ nodes and the total number of computational cells for the whole domain amounting over 1.7 mln.

A direct numerical simulation allows for an unbiased analysis of the turbulent flow to extract physical fluctuations and to perform user-defined averaging

of the flow. The optimal time step of the simulation was estimated by performing several computational tests. It was found to be of the order of 10^{-7} s. Using this time step, it was possible to obtain a sequence of solutions for about 10 ms flow time only. Analysing the obtained results, it appeared that velocity fluctuations within the gap are relatively small. Their initial amplitude at the gap entrance was below 1% and increased to about 8% at the gap exit. The DNS solution confirmed the experimental findings for the quasi laminar flow within the gap and the early transition at the gap exit.

Figure 6 shows velocity fluctuations extracted from the DNS simulations for three selected points behind the processing element. It can be found that the flow in the vicinity of the upper wall is characterized by nearly regular high amplitude turbulent fluctuations with a period of about 0.2 ms. They represent small scale vortices created in the turbulent boundary layer separating from the gap exit. The reversal flow present closer to the channel symmetry plane exhibits low frequency variation of its amplitude. Here, the flow is mainly concentrated in a large vortex with slowly varying in time and space location. Such behaviour can be well visualized by constructing a short movie from the sequence of DNS solutions.

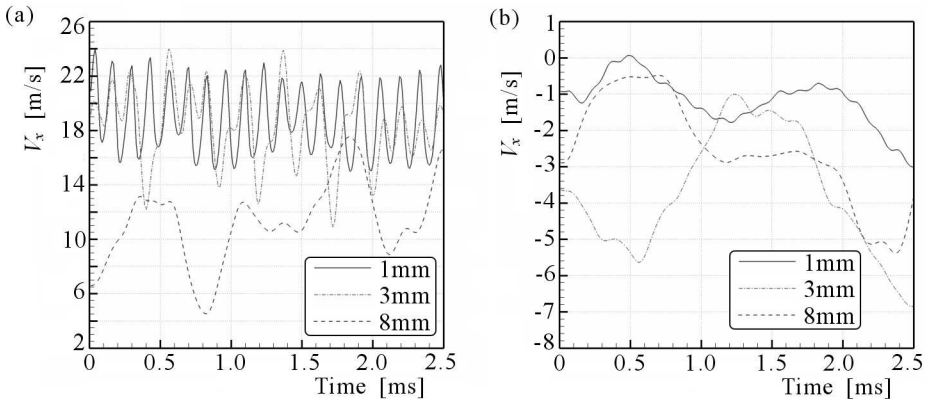


Fig. 6. Direct numerical simulation. Temporal variation of the streamwise velocity component monitored for the central plane at three selected locations behind the gap ($x = 1$ mm, 3 mm and 8 mm); (a) $y = -0.2$ mm; (b) $y = -2.0$ mm

The averaged flow characteristics close to the top wall were well reproduced using about 200 time steps, i.e. by averaging turbulent fluctuations over 2 ms time interval. This averaging time was selected as a compromise necessary to limit the total computational time. The main features of the averaged velocity fields obtained from the DNS flow simulation were in a good agreement with the experimental findings. It was confirmed that upstream the gap the average flow velocity was about 5 m/s, and in the gap a strong acceleration of the flow occurs with velocity peak values reaching about 23 m/s.

Numerical simulation allows for evaluation of all three components of the velocity fluctuations, however for comparison of the obtained results with the experimental data, a two-dimensional projection of the flow field was used. Hence, the mean square value of the velocity fluctuations V'_x and V'_z obtained from the direct numerical simulation were used to evaluate $tk_{e_{xz}}$ representing the turbulent kinetic energy in the similar way as in the experimental part.

Figure 7 displays $tk_{e_{xz}}$ obtained for a relatively short averaging time. It indicates that the flow turbulence, i.e. the averaged velocity fluctuations reach their maximum about 6 mm behind the gap. It is in relatively good agreement with the experimental data obtained from the PIV measurements (comp. Fig. 5 – P5).

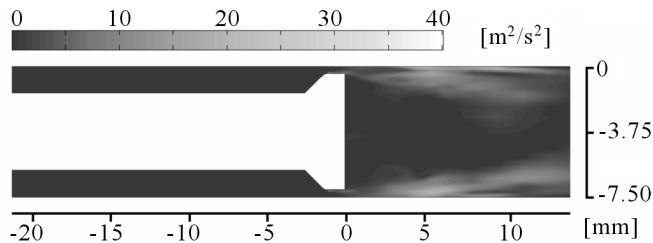


Fig. 7. Direct numerical simulation. Contours of the mean square value of the velocity fluctuations $tk_{e_{xz}}$ calculated from 200 time steps. Visible asymmetry of the contours is due to short averaging time (2 ms)

Direct numerical simulations utilize large amount of computer resources and computational time. The analysis performed using the averaged turbulent model applied to one-quarter of the cavity, confirms main features of the flow field obtained by direct numerical simulation. The average velocity vector field attains the maximum value of about 20 m/s in the gap between the processing element and the top wall, and a well developed recirculation region is present behind the gap. However, assuming in the numerical model turbulent flow at the channel inlet implies its fast development within the gap. Hence, the averaged turbulent model predicts highly developed turbulent flow already within the gap, contrary to the experimental observations.

A comparison of the numerical and experimental results for the averaged velocity profiles was done to validate the numerical simulations. Figure 8 combines the profiles of the x -component of the velocity obtained from the numerical simulations using the turbulent model (gray line), the direct numerical simulation (solid line), and micro-PIV measurements (circles). Each experimental point represents the space and time averaged velocity value evaluated as it was described above. The DNS numerical data are single point averages over 2.5 ms flow time. The numerical and experimental profiles are

compared at three locations behind the processing element: 1 mm (Fig. 8 – P3), 3 mm (Fig. 8 – P4), and 8 mm (Fig. 8 – P5). Qualitative agreement of

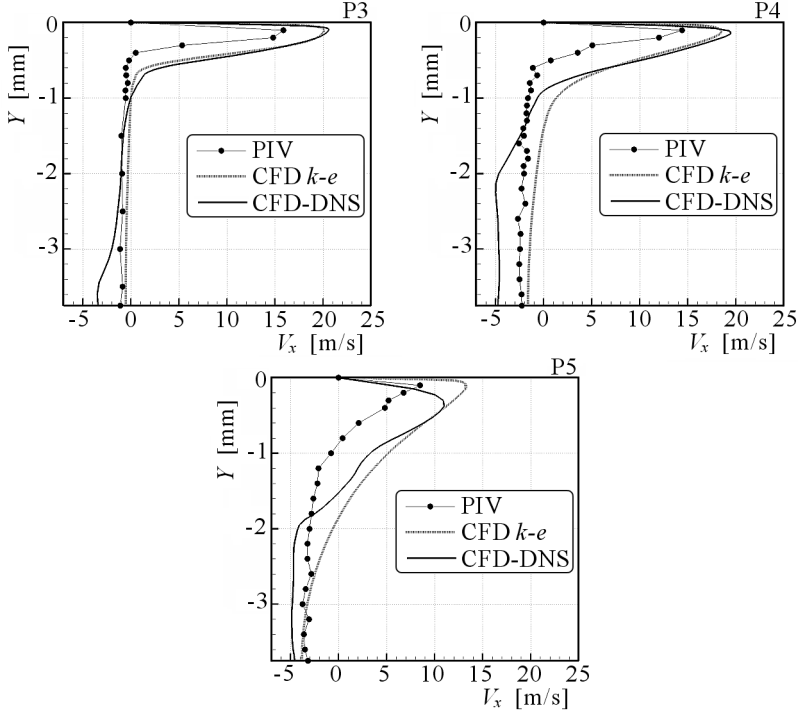


Fig. 8. Comparison of the numerical and experimental longitudinal velocity profiles evaluated along the channel depth from the top wall to the channel axis. Three locations interrogated experimentally are displayed: (P3) – 1 mm, (P4) – 3 mm, and (P5) – 8 mm behind the processing element. Black circles indicate averaged PIV measured data; gray line indicates CFD $k-\epsilon$ data from the $k-\epsilon$ turbulent numerical model; solid line indicates CFD-DNS averaged data from direct numerical simulations

the numerical and experimental results in the vicinity of the processing element is fairly good. The presence of strong velocity gradients close to the top wall is probably responsible for diminishing of the resolution of the PIV evaluation, which in turn decreases in all three cases the peak magnitude of the measured velocity profile. The negative velocities close to the flow axis indicate the reversal flow, confirmed in both numerical profiles. However, a more detailed analysis of these results shows significant differences – the local flow rates calculated from the experimental data along profiles P3-P4 is much lower than the numerical prediction. For the profiles located 8 mm behind the processing element (Fig. 8 – P5), the difference between numerical and experimental results becomes even more significant, although the location of the velocity maximum is still relatively well preserved. There are several factors

responsible for the obvious discrepancies between the experimental and numerical profiles. First of all, it must be noted that the analysed turbulent flow is strongly three-dimensional and the flow measurements performed at few points cannot properly represent the average flow field across the channel. It is particularly true for the fluctuating recirculation flow present behind the processing element. Hence, fluxes calculated using only one-component velocity profile are not representative, and as it is seen in Fig. 8 it leads to serious deviations. The DNS simulation indicates strong temporal flow field fluctuations with a broad range of characteristic frequencies (Fig. 6). Therefore, it was difficult to obtain a representative averaging time for the DNS simulation, and the time interval of 2.5 ms used to obtain the averages is most probably insufficient, as it is already indicated by slight asymmetry of the fluctuation contours in Fig. 7.

Evaluation of velocity field fluctuations may permit one to identify flow regions responsible for the droplets break-up in the emulsifier. In the turbulent flow, the droplets break-up rate is related to the magnitude of the kinetic energy dissipation. Distribution of the turbulent kinetic energy, obtained from the direct numerical simulations shows that the maximum value of turbulent kinetic energy is reached in the region just behind the processing element. It is where the intense mixing of the high velocity fluid ejected from the gap with a low velocity of the recirculating flow behind the processing element takes place. It is in agreement with the experimental findings indicating the highest velocity fluctuation about 8 mm behind the gap. However, the k - ϵ turbulent numerical model points out that the maximum of turbulent energy dissipation rate is at the gap entry, where both direct numerical simulation and micro-PIV experiment indicate a very little amplitude of velocity fluctuations. The conclusion would be that the assumption of turbulence in numerical modelling may give misleading results, especially in regions too small to allow for its development.

4. Conclusions

Velocity measurements (micro-PIV) indicated almost a uniform velocity flow field in the short micro-channel formed by the gap region of the emulsifier. It means that the turbulence is still not fully developed. A strong recirculation zone with the reversal of flow is found behind the processing element. The turbulent fluctuations of the velocity field and break-up of the flow symmetry observed in this region indicate that probably transition from the laminar to turbulent flow regime occurs there. Numerical modelling confirmed main details of the velocity flow field measured by the micro-PIV method. The DNS

and turbulent flow models were successfully applied producing a similar averaged flow structure. Although, the turbulent flow model overestimates early turbulent transition within the gap. The DNS model confirms the observed delayed transition to turbulence within short contraction of the emulsifier. However, computational overload of the DNS simulations (about 1month for 2 ms flow time) prohibited deeper quantitative analysis of the flow pattern. It appears necessary to extend computational time and largely expand the area covered by the experimental interrogation to explain in details the observed discrepancies of measured and computed velocity profiles.

Acknowledgments

This investigation was conducted in the framework of EMMA project supported by Austrian Ministry of Science and Education, contract no.: GZ 45.534/1-VI/6a/2003 CONEX. The micro-PIV expertise was developed in the framework of EU Thematic Network PIVNET2.

References

1. BRENN G., 2005, Emulsions with nanoparticles for new materials, *Scientific Report of EMMA Project*, Graz University of Technology, TU Graz
2. BŁOŃSKI S. KORCZYK P, KOWALEWSKI T.A., 2007, Analysis of turbulence in a micro-channel emulsifier, *Int. J. Thermal Scs*, doi:10.1016/j.ijthermalsci.2007.01.028
3. Fluent 6.3, 2006, *Users Guide*, Fluent Inc., Lebanon NH, USA.
4. 4. KOWALEWSKI T.A., BŁOŃSKI S. KORCZYK P., 2006, Turbulent flow in a microchannel, *Proc. of ASME ICNMM2006*, CD-ROM paper 96090, Limerick, Ireland
5. LI H., OLSEN G., 2006, MicroPIV measurements of turbulent flow in square microchannels with hydraulic diameters from 200 μm to 640 μm , *Int. J. Heat Fluid Flow*, **27**, 123-134
6. MEINHART C.D., WERELEY S.T., GRAY M.H.B., 2000, Volume illumination for two-dimensional particle image Velocimetry, *Measurement Science and Technology*, **11**, 809-814
7. SANTIAGO J.G., WERELEY S.T., MEINHART C.D., BEEBE D.J., ADRIAN R.J., 1998, A micro particle image Velocimetry system, *Exp. Fluids*, **25**, 316-319
8. SHINOHARA K., SUGII Y., AOTA A., HIBARA A., TOKESHI M., KITAMORI T., OKAMOTO K., 2004. High-speed micro-PIV measurements of transient flow in microfluidic devices, *Measurement Science and Technology*, **15**, 1965-1970

9. STEINER H., TEPPNER R., BRENN G., VANKOVA N., TCHOLAKOVA S., DENKOV N., 2006, Numerical simulation and experimental study of emulsification in a narrow-gap homogenizer, *Chemical Engineering Science*, **61**, 5841-5855

Analiza przepływu turbulentnego w mikro-kanale przy wykorzystaniu cyfrowej anemometrii obrazowej

Streszczenie

W pracy przedstawiono analizę turbulentnego przepływu wody przez mikro-kanal emulsyfikatora. Wyniki uzyskane eksperymentalną techniką Cyfrowej Anemometrii Obrazowej (PIV – *Particle Image Velocimetry*) zaadoptowanej do pomiarów w mikro-skali (micro-PIV) porównano z wynikami symulacji numerycznych przeprowadzonych zarówno poprzez bezpośrednie rozwiązanie równań Naviera-Stokesa (DNS – *Direct Numerical Simulation*), jak i wykorzystując hipotezę Reynoldsa uśredniającą fluktuacje prędkości i ciśnienia (model $k-\varepsilon$). Część eksperymentalna pracy przeprowadzona została na unikalnym stanowisku pomiarowym bazującym na mikroskopii epi-fluorescencyjnej i szybkim obrazowaniu analizowanego przepływu. Charakterystyki przepływu wyznaczone eksperymentalnie i numerycznie symulacją DNS wykazały, że turbulizacja przepływu pojawia się dopiero w końcowym przekroju mikro-kanalu, osiągając maksimum w kanale wylotowym emulsyfikatora.

Manuscript received February 9, 2007; accepted for print March 19, 2007